Supporting Information

Mix and Match – Controlling the Functionality of Spin-Crossover Materials Through Solid Solutions and Molecular Alloys

Malcolm A. Halcrow*

School of Chemistry, University of Leeds, Woodhouse Lane, Leeds, UK LS2 9JT.
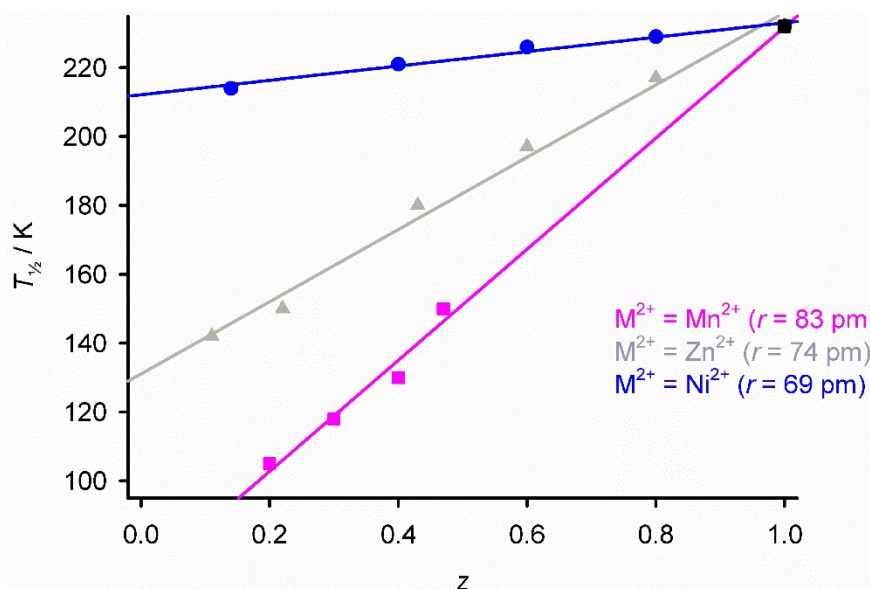*E-mail: m.a.halcrow@leeds.ac.uk.*

Figure S1 Variation of $T_{1/2}$ with composition in $[Fe_zM_{1-z}(3\text{-bpp})_2][NCSe]_2$ (3-bpp = 2,6-*bis*{1*H*-pyrazol-3-yl}pyridine, a regioisomer of the 1-bpp ligand in Scheme 1 of the main article) with different dopant ions: M = Mn (■), Zn (▲) and Ni (●). Data for each dopant are linked by a regression line for clarity. The Figure is modified from ref. 1 (copyright the Royal Society of Chemistry), and contains data from refs. 2-4.

All the dopant ions lower $T_{1/2}$, in the order: M = Mn > Zn > Ni. That is the trend predicted from the ionic radii of the dopant ions (shown). Larger dopant ions lead to expansion of the lattice, thus reducing the chemical pressure about each iron centre. That stabilises the larger high-spin form of the iron complex (r = 78 pm) and reduces $T_{1/2}$, as observed.
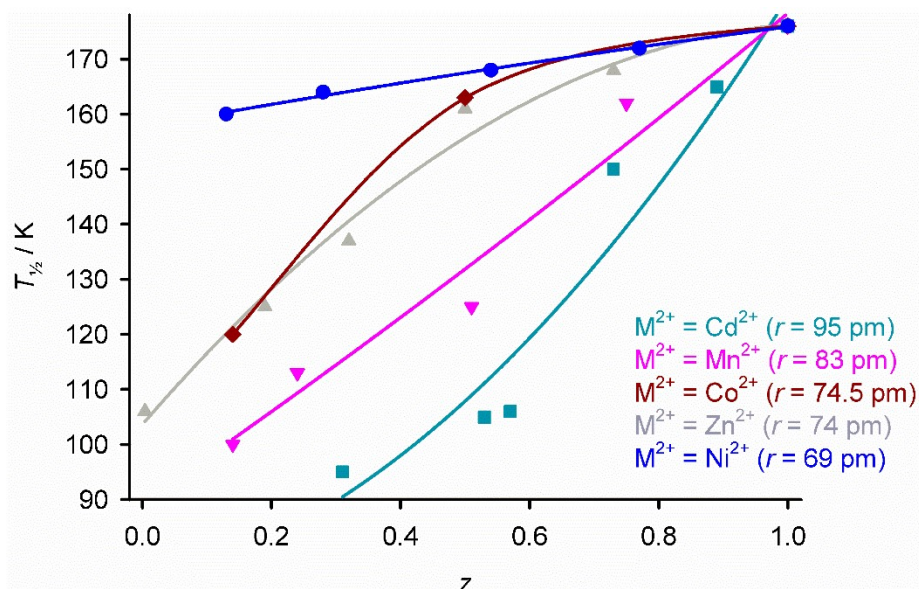
Figure S2 Variation of $T_{1/2}$ with composition in $[Fe_zM_{1-z}(NCS)_2(phen)_2]$ (phen = 1,10-phenanthroline) with different dopant ions: M = Cd (■), Mn (▼), Zn (▲), Co (♦) and Ni (●). Data for each dopant are linked by a regression curve for clarity. Data are replotted from refs. 5-7.

Some of these literature data are more scattered than for Figure S1, but it is clear that the dopant's influence on $T_{1/2}$ also correlates with the dopant ionic radius in this system.

Table S1. Molecular SCO materials containing isomorphous or non-isomorphous dopant ions, that have been used to study or manipulate SCO cooperativity, or to introduce other functionality. Other examples containing trace quantities of dopants are listed in Table S4.

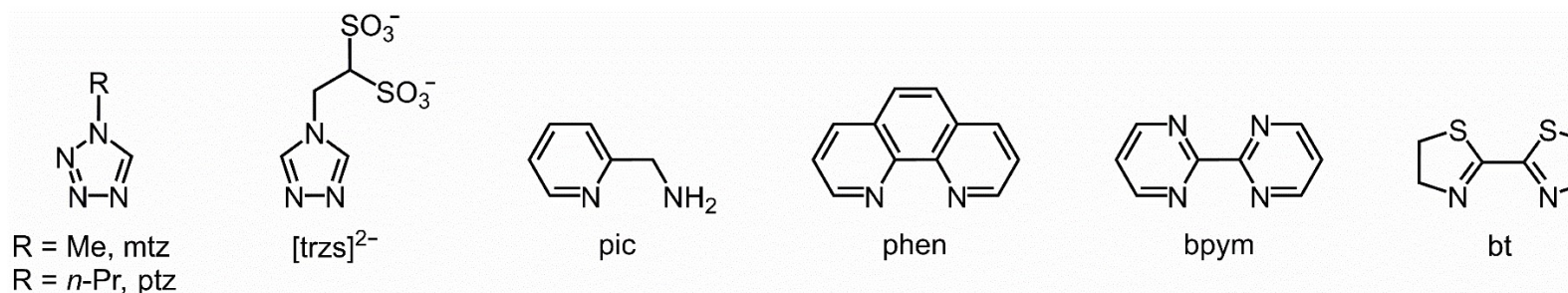| Compound[a]	SCO $T_{1/2}$; form	Dopant	Notes	Refs.
[Fe(mtz)$_6$][ClO$_4$]$_2$	66 K; gradual, 50% complete	Zn	The crystal contains two unique high-spin Fe environments, only one of which undergoes SCO.	8
		Ni	Fe$_{0.35}$Ni$_{0.65}$ exhibits complete SCO with an unsymmetric hysteresis, implying a phase transition occurs below 60 K.	9
[Fe(ptz)$_6$][BF$_4$]$_2$	125 or 131 K; abrupt, 7 K hysteresis	Zn	$T_{1/2}$ depends on scan rate because of a kinetically slow phase change. The phase change does not occur with more than *ca* 70% Zn doping.	10-14
		Ru		15, 16
[Fe(NCS)$_2$(phen)$_2$]	179 K; abrupt	Zn	The LIESST relaxation temperature did not vary upon Zn doping across the complete concentration range.[b]	5-7, 17, 18
		Mn	Increased doping makes SCO progressively less complete as $T_{1/2}$ is lowered.	5
		Co		5
		Ni	The LIESST relaxation temperature decreases measurably with increased Ni doping.[b]	5, 7
		Cd	The LIESST relaxation temperature increases measurably with increased Cd doping, which is the opposite trend to the Ni-doped materials.[b]	7
[Fe(NCS)$_2$(dppz)$_2$]·py	143 K; abrupt, 40 K hysteresis	Mn	Increased doping makes SCO progressively less complete as $T_{1/2}$ is lowered, until the material remains high-spin at 12% Mn. Intermediate compositions show TIESST on thermal cycling.[c]	19
[Fe(pic)$_3$]Cl$_2$·MeOH	153 K; gradual	Zn		20
		Co		20
[Fe(pic)$_3$]Cl$_2$·EtOH	114 and 121 K; abrupt, 2 steps	Zn	Stepped transition reflects an intermediate mixed-spin crystal phase that exists at 50% conversion. The intermediate phase and step are not observed with >10% Zn doping.	21-27
		Co		28
[Fe(1-bpp)$_2$][BF$_4$]$_2$	261 K; abrupt, 3 K hysteresis	Zn		1, 29
		Co	The LIESST relaxation temperature did not vary upon Co doping within the concentration range examined (up to 23% Co).[b]	30
		Ni		1, 29, 31
		Ru		1
[Fe(1-bpp)$_2$][ClO$_4$]$_2$	Complex is high-spin	Ni	The Fe and Ni precursor complexes are not isomorphous. The 26% Ni-doped material exhibits complete, abrupt SCO at $T_{1/2}$ = 251 K.	32

Table S1 continued.

Compound[a]	SCO $T_{1/2}$; form	Dopant	Notes	Refs.
[Fe(1-bpp^{COOH})$_2$][ClO$_4$]$_2$	383 K; abrupt, 3 K hysteresis	Co	The Fe and Co precursor complexes are not isomorphous. The 8% Co-doped material is not an SIM at low temperatures.[d]	33
[Fe(3-bpp)$_2$][BF$_4$]$_2$	176 K; abrupt, 10 K hysteresis	Mn	Increased doping makes SCO progressively less complete as $T_{1/2}$ is lowered, until the material is almost high-spin at 15% Mn. The 10% Mn sample shows TIESST on thermal cycling.[c]	34, 35
[Fe(3-bpp)$_2$][NCSe]$_2$	231 K; abrupt, 2 K hysteresis	Zn Ni Mn	The LIESST relaxation temperature increases slightly with increased Zn doping[b] The LIESST relaxation temperature decreases slightly with increased Ni doping, which is the opposite trend to the Zn-doped materials.[b] Increased doping makes SCO progressively less complete as $T_{1/2}$ is lowered, until the material remains high-spin at 80% Mn. The LIESST relaxation temperature increases slightly with increased Mn (as in the Zn-doped samples).[b]	2 3 4
[Fe(Me1,3-bpp)$_2$][ClO$_4$]$_2$	184 K; abrupt	Zn	≥36% Zn doping makes SCO progressively less complete as $T_{1/2}$ is lowered. Samples containing less Zn were not studied in detail.	36
[Fe(qnal)$_2$]·CH$_2$Cl$_2$	218 K; abrupt, 2 K hysteresis	Zn Ni		37 37
[Fe(NCS)$_2$(bapbpy)]	183 and 237 K; abrupt, 2 steps, 22 K and 4 K hysteresis	Zn	Stepped transition reflects a sequence of two crystallographic phase transitions during the SCO process. The step is not observed with ≥24% Zn doping.	38
[Fe(NCBH$_3$)$_2$(^{2Me}L)]	Complex is high-spin	Zn Ni	The Zn-doped compound remains high-spin. Doping with >50% Ni reveals an abrupt spin-transition at 72 K, which is kinetically inhibited in the undoped material.	39 39
[Fe(Py$_2$-C)][ClO$_4$]$_2$·H$_2$O	141 K; gradual	Co	The 60% Co-doped material is a field-induced SIM at low temperature, but did not exhibit a LIESST effect.[b,d]	40
[Fe(CN)$_2$(N$_3$O$_2$)]	210 and 155 K; abrupt, ca 27 K and 10 K hysteresis	Mn	The pure Fe complex shows a complicated interplay between two SCO processes, reflecting a kinetically slow Fe−O bond breaking/formation step. Doping with 5% Mn almost quenches the thermal SCO by stabilising the 7-coordinate isomer.	41
[Fe({MePy}$_3$tren)][PF$_6$]$_2$	215 K; gradual	Zn	Zn doping has an unusually small effect on the thermal SCO.	42
[Fe({MePy}$_3$tren)][PF$_6$]$_2$·MeCN	Not reported	Zn	A crystal containing 0.5% Fe exhibited gradual SCO at $T_{1/2}$ = 125 K.	43

Table S1 continued.

Compound[a]	SCO $T_{1/2}$; form	Dopant	Notes	Refs.
[{Fe(NCS)$_2$(bt)}$_2$(μ-bpym)]	197 K (gradual) and 163 K (abrupt)	Zn	The dinuclear Fe complex exhibits two-step SCO *via* a discrete HS:LS intermediate state. Doping with 85% Zn converts this to a gradual transition with no intermediate step.	44
[Me$_2$NH$_2$]$_6$[Fe$_3$(μ-trzs)$_6$(H$_2$O)$_6$]	355 K; abrupt, 90 K hysteresis	Zn	The linear trinuclear Fe$_3$ complex exhibits SCO at its central Fe atom, with an exceptionally high-temperature TIESST effect.[c] The hysteresis and TIESST are retained upon Zn doping, showing they are a property of the individual molecules not the solid lattice.	45
[Co(terpyOC$_{16}$H$_{33}$)$_2$][BF$_4$]$_2$	239 K; reverse-SCO;[e] abrupt, 43 K hysteresis	Zn	Doping with Zn stabilises the low-temperature, high-spin form of the reverse-SCO lattice[e] and increases $T_{1/2}$ without narrowing the hysteresis loop.	46
		Fe	Doping with Fe stabilises the high-temperature, low-spin form of the reverse-SCO lattice[e] and lowers $T_{1/2}$ without narrowing the hysteresis loop. The 20% Fe sample shows TIESST on thermal cycling.[c]	46, 47

[a]1-bpp = 2,6-*bis*{pyrazol-1-yl}pyridine; 1-bpp^{COOH} = [2,6-*bis*{pyrazol-1-yl}pyrid-4-yl]carboxylic acid; ^{2Me}L = *N,N'*-dimethyl-*N,N'*-*bis*-{pyrid-2-ylmethyl}-1,2-diaminoethane; 3-bpp = 2,6-*bis*{1*H*-pyrazol-3-yl}pyridine; bapbpy = *N*6,*N*6'-di(pyridin-2-yl)-2,2'-bipyridine-6,6'-diamine; bpym = 2,2'-bi(pyrimidine); bt = 2,2'-bi(thiazoline); dppz = dipyrido[3,2-*a*:2'3'-*c*]phenazine; mtz = 1-methyltetrazole; Me1,3-bpp = 2-{3-methylpyrazol-1-yl}-6-{1*H*-pyrazol-3-yl}pyridine; {MePy}$_3$tren = t*ris*{4-(6-methylpyrid-2-yl)-3-azabutenyl}amine; N$_3$O$_2$ = 2,13-dimethyl-6,9-dioxa-3,12,18-triazabicyclo[12.3.1]-octadeca-1(18),2,12,14,16-pentaene; phen = 1,10-phenanthroline; pic = 2-(aminomethyl)pyridine; ptz = 1-*n*-propyltetrazole; py = pyridine; Py$_2$-C = 1,8-bis(pyridin-2-ylmethyl)-1,4,8,11-tetraazacyclotetradecane; Hqnal = *N*-(quinol-8'-yl)-2-hydroxy-1-naphthaldimine; terpyOC$_{16}$H$_{33}$ = 4'-hexadecoxy-2,2':6',2''-terpyridine; [trzs]$^{2-}$ = 2-(1,2,4-triazol-4-yl)ethane-1,1-disulfonate. [b]LIESST = light-induced excited spin state trapping (ref. 143). [c]TIESST = thermally induced excited spin state trapping (ref. 144). [d]SIM = single ion magnet (ref. 145). [e]Reverse-SCO is a low→high-spin transition on cooling (ref. 146).

Scheme S1. Ligands listed in Table S1.

dppz

1-bpp

1-bpp^{COOH}

3-bpp

Me1,3-bpp

terpyOC$_{16}$H$_{33}$

Hqnal

bapbpy

^{2Me}L

N$_3$O$_2$

Py$_2$-C

{MePy}$_3$tren
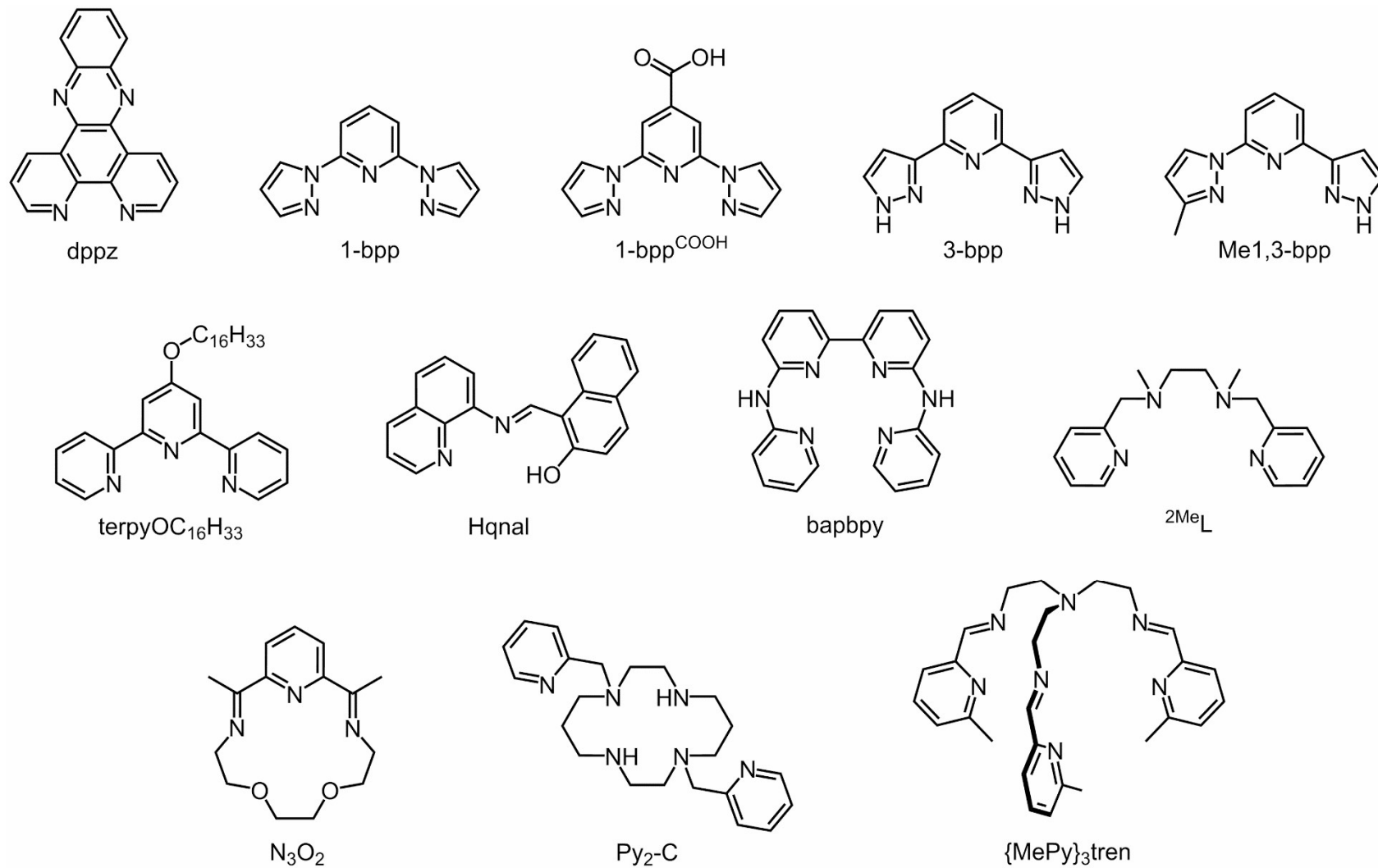
Scheme S1 continued.

Table S2. Coordination polymer SCO materials containing isomorphous or non-isomorphous dopants, that have been used to study or manipulate SCO cooperativity. Other examples containing trace quantities of dopants are listed in Table S4.

Compound[a]	SCO $T_{1/2}$; form	Dopant	Notes	Refs.
[Fe(μ-atrz)$_3$][NO$_3$]$_2$	328 K; abrupt, 37 K hysteresis	Zn Ni Mn	1D coordination polymer.	48-53 53-55 53
[Fe(μ-atrz)$_3$][CH$_3$SO$_3$]$_2$	281 K; abrupt, 15 K hysteresis	Zn	1D coordination polymer. A sample containing 10% Fe was used to probe the vibrational structure of this material by inelastic neutron scattering.	56
[Fe(μ-Htrz)$_3$][NO$_3$]$_2$·H$_2$O	350 K; abrupt, 10 K hysteresis	Ni	1D coordination polymer.	57
[Fe(μ-trz)(μ-Htrz)$_2$]BF$_4$	365 K; abrupt, 40 K hysteresis or 333 K; abrupt, 20 K hysteresis	Zn	1D coordination polymer, which can be crystallised in two SCO-active polymorphs. Zn doping has been used to tune $T_{1/2}$ in nanoparticles of this material.	58-61
[Fe(μ-endi)$_3$][BF$_4$]$_2$	143 K; gradual	Zn	1D coordination polymer. The LIESST relaxation temperature increases slightly with increased Zn doping.[b]	62, 63
[Fe(μ-btzp)$_3$][BF$_4$]$_2$	158 K; gradual	Zn	1D coordination polymer. The LIESST relaxation temperature increases slightly with increased Zn doping.[b]	62, 63
[Fe(NCS)$_2$(μ-btr)$_2$]·H$_2$O	134 K; abrupt, 21 K hysteresis	Zn Ni Co	2D coordination polymer.	64-66 65-70 65, 70-72
[Fe(μ-bbtr)$_3$][ClO$_4$]$_2$	105 K; abrupt, 8 K hysteresis	Zn	2D coordination polymer, which undergoes a phase change just above $T_{1/2}$. Zn doping makes SCO progressively less complete as $T_{1/2}$ is lowered.	73-77
[Fe(μ-pyz){Pd(CN)$_4$}]	296 K; abrupt, 12 K hysteresis	Zn Ni Co Mn	3D porous metal-organic framework	78 78 78 78
[Fe(μ-pyz){Pt(CN)$_4$}]	295 K; abrupt, 26 K hysteresis	Zn Ni Co	3D porous metal-organic framework	79 80 80
[Fe(μ-pyz){Fe(CN)$_5$(NO)}]	265 K; abrupt, 40 K hysteresis	Ni Co	3D coordination polymer.	81 81

Table S2 continued.

Compound[a]	SCO $T_{1/2}$; form	Dopant	Notes	Refs.
[Fe(μ-PyCCPy){Au(CN)$_2$}$_2$]	224 K; abrupt, 5 K hysteresis	Ni	3D coordination polymer. Ni doping makes the abrupt SCO more continuous (gradual), revealing colossal thermal expansion about the SCO temperature range.	82
[Fe(μ_3-ta)$_2$]	524 K; abrupt, 117 K hysteresis	Cu	[Fe(ta)$_2$] and [Cu(ta)$_2$] are isomorphous but can't be co-crystallised from solution. Ball milling mechanical mixtures of [Fe(ta)$_2$] and [Cu(ta)$_2$] yielded a homogeneous solid solution material, but whose SCO was not investigated.	83

[a]atrz = 4-amino-1,2,4-triazole; bbtr = 1,4-bis(1,2,3-triazol-1-yl)butane; btr = 4,4'-bi(1,2,4-triazole); btzp = 1,2-*bis*({tetrazol-1-yl}propane; endi = 1,2-*bis*({tetrazol-1-yl}ethane; PyCCPy = *bis*(pyrid-4-yl)ethyne; pyz = pyrazine; Hta = 1*H*-1,2,2-triazole; Htrz = 4*H*-1,2,4-triazole. [b]LIESST = light-induced excited spin state trapping (ref. 143).
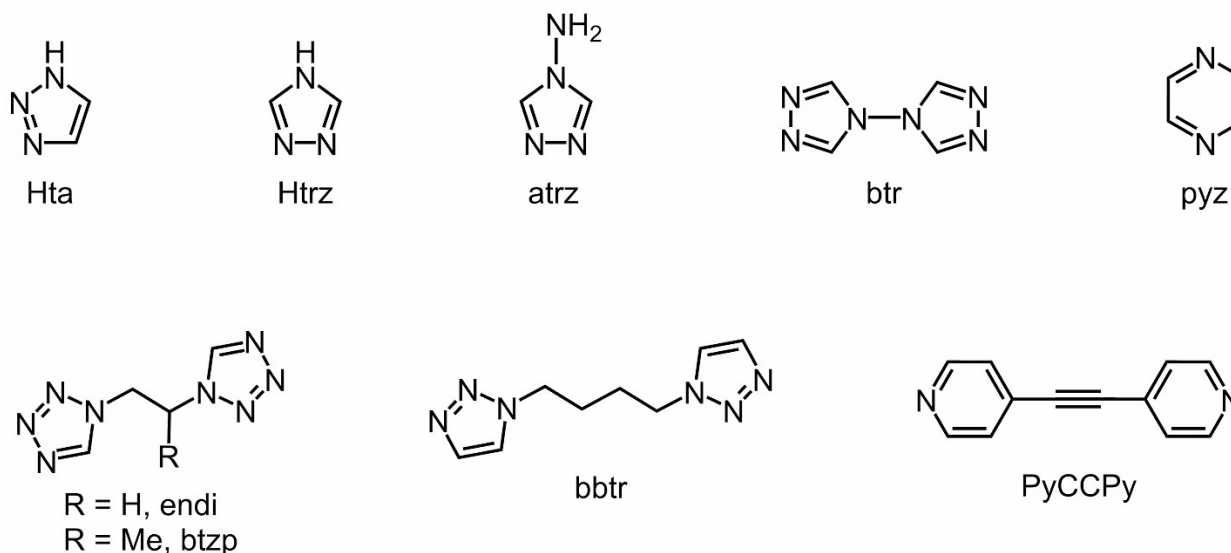
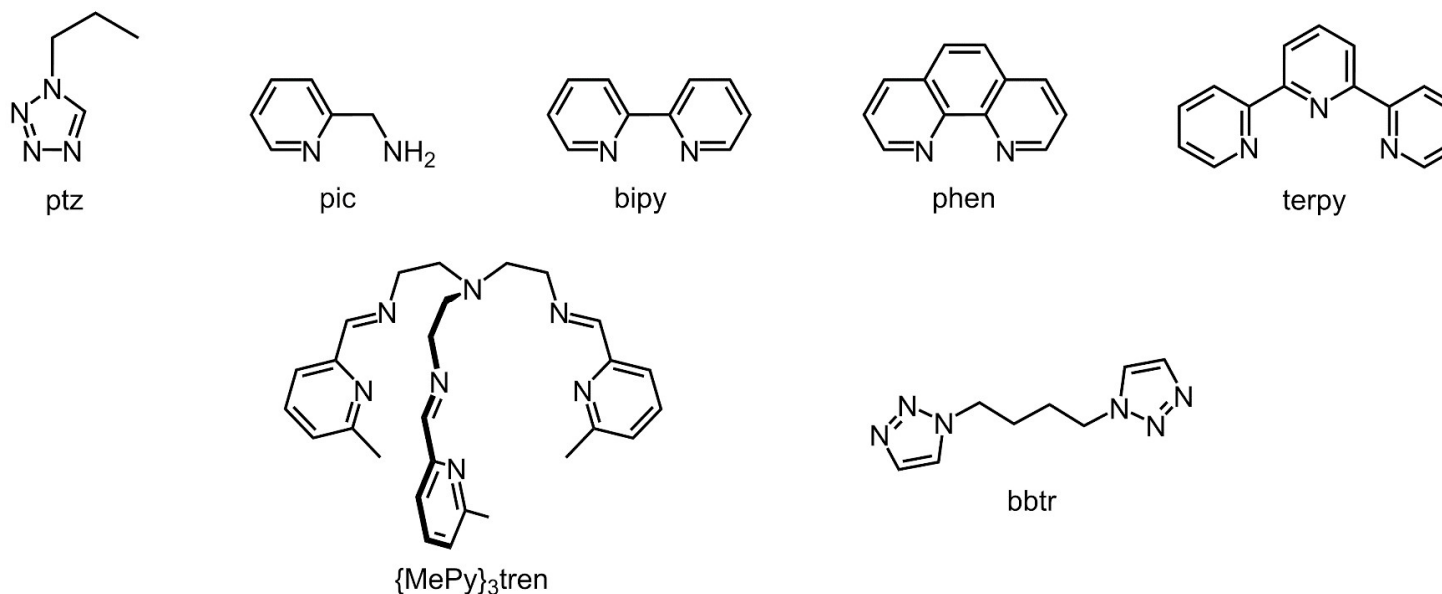**Scheme S2.** Ligands listed in Table S2.

Table S3. Highly dilute solid solutions of iron(II) complexes in inert host crystals, used to study the photophysics of isolated molecules in the solid state.

Compound[a]	SCO $T_{1/2}$; form	Host lattice metal ion	Notes	Refs.
$[Fe(ptz)_6][BF_4]_2$	125 or 131 K; abrupt, 7 K hysteresis	Zn	$T_{1/2}$ depends on scan rate because of a kinetically slow phase change. Crystals containing ≥0.5% Fe were used to probe isolated iron sites in the lattice.	12
$[Fe(bipy)_3][ClO_4]_2$	Complex is low-spin	Zn	Crystals containing 0.5% Fe were still low-spin, and were used to probe the photophysics of isolated iron sites in the lattice.	84
		Ni	Crystals containing 0.5% Fe were still low-spin, and were used to probe the photophysics of isolated iron sites in the lattice.	84
		Mn	Crystals containing 0.5% Fe were still low-spin, and were used to probe the photophysics of isolated iron sites in the lattice.	84
$[Fe(bipy)_3][PF_6]_2$	Complex is low-spin	Zn	Crystals containing 0.01-1% Fe were still low-spin, and were used to probe the photophysics of isolated iron sites in the lattice.	85-87
		Mn	Crystals containing 0.01-1% Fe were still low-spin, and were used to probe the photophysics of isolated iron sites in the lattice.	86, 87
		Co	Highly dilute crystals were still low-spin, and were used to probe the photophysics of isolated iron sites in the lattice.	87
		Cd	Crystals containing 0.01-1% Fe were still low-spin, and were used to probe the photophysics of isolated iron sites in the lattice.	86, 87
$[Fe(phen)_3][ClO_4]_2$	Complex is low-spin	Zn	Crystals containing 0.5% Fe were still low-spin, and were used to probe the photophysics of isolated iron sites in the lattice.	84
		Ni	Crystals containing 0.5% Fe were still low-spin, and were used to probe the photophysics of isolated iron sites in the lattice.	84
		Mn	Crystals containing 0.5% Fe were still low-spin, and were used to probe the photophysics of isolated iron sites in the lattice.	84
$[Fe(pic)_3]Cl_2 \cdot MeOH$	153 K; gradual	Zn	Crystals containing 0.05% Fe were used to probe the photophysics of isolated iron sites in the lattice.	88
		Mn	Crystals containing 0.05% Fe were used to probe the photophysics of isolated iron sites in the lattice.	88
$[Fe(pic)_3]Cl_2 \cdot EtOH$	114 and 121 K; abrupt, 2 steps	Zn	Stepped transition reflects an intermediate mixed-spin crystal phase that exists at 50% conversion. Crystals containing 0.05% Fe were used to probe the photophysics of isolated iron sites in the lattice.	88
		Mn	Crystals containing 0.05% Fe were used to probe the photophysics of isolated iron sites in the lattice.	88

Table S3 continued.

Compound[a]	SCO $T_{1/2}$; form	Host lattice metal ion	Notes	Refs.
[Fe(terpy)$_2$][ClO$_4$]$_2$	Complex is low-spin	Mn	A sample containing 2% Fe was still low-spin but exhibited a LIESST effect, which is not shown by the pure Fe complex.[b]	89
[Fe({MePy}$_3$tren)][PF$_6$]$_2$	215 K; gradual	Zn	Crystals containing 0.31 and 0.05% Fe were used to probe the photophysics of isolated iron sites in the lattice.	42, 90
[Fe({MePy}$_3$tren)][PF$_6$]$_2$·MeCN	Not reported	Zn	A crystal containing 0.5% Fe was used to probe the photophysics of isolated iron sites in the lattice.	43
[Fe(μ-bbtr)$_3$][ClO$_4$]$_2$	105 K; abrupt, 8 K hysteresis	Zn	2D coordination polymer, which undergoes a phase change just above $T_{1/2}$. Samples containing 2-10% Fe remain high-spin on cooling, and were used to probe the photophysics of isolated iron sites in a solid lattice.	91, 92

[a]bipy = 2,2'-bipyridine; bbtr = 1,4-bis(1,2,3-triazol-1-yl)butane; {MePy}$_3$tren = *tris*{4-(6-methylpyrid-2-yl)-3-azabutenyl}amine; phen = 1,10-phenanthroline; pic = 2-(aminomethyl)pyridine; ptz = 1-*n*-propyltetrazole; terpy = 2,2':6',6''-terpyridine.   [b]LIESST = light-induced excited spin state trapping (ref. 143).

ptz   pic   bipy   phen   terpy

{MePy}$_3$tren   bbtr

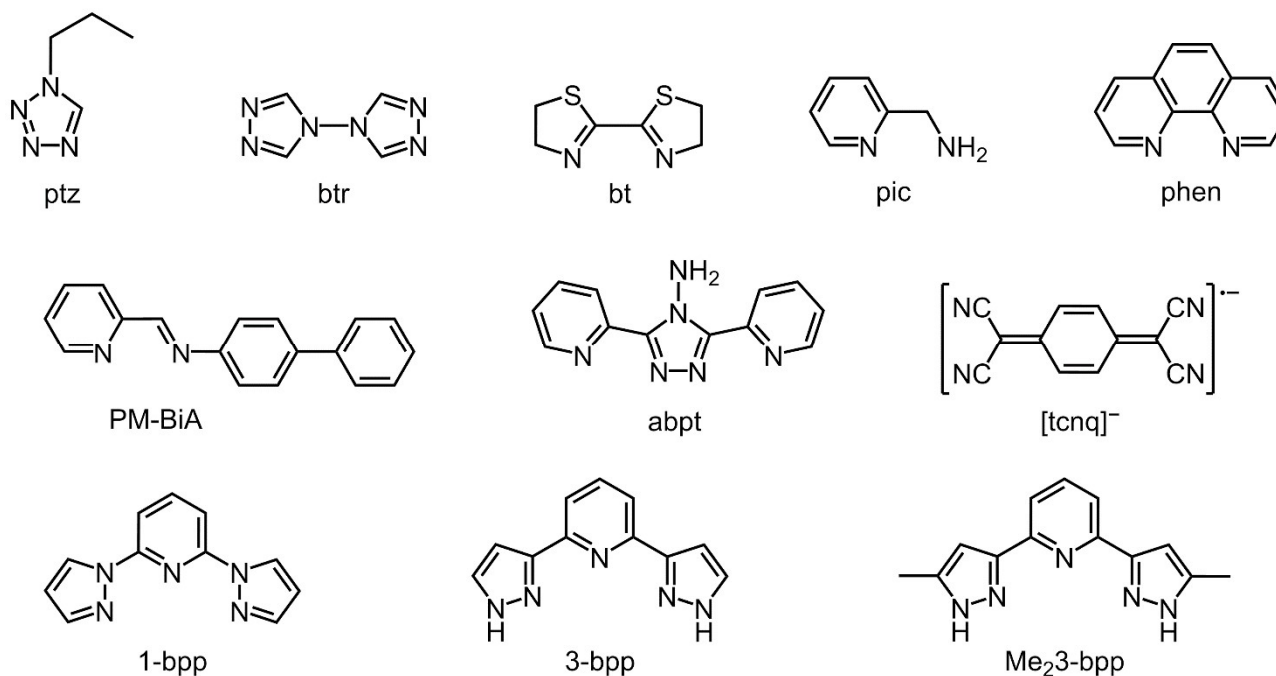**Scheme S3.** Ligands listed in Table S3.

Table S4. SCO materials containing trace paramagnetic dopant ions, that have been used to probe SCO by EPR spectroscopy.

Compound[a]	SCO $T_{1/2}$; form	Dopant	Notes	Refs.
$[Fe(ptz)_6][BF_4]_2$	125 or 131 K; abrupt, 7 K hysteresis	Mn	1-2% Mn dopant used as an EPR probe of the iron spin state during thermal SCO. Distinguished the two different low-spin phases accessible in the low-spin state (Table S1).	93
		Cu	1-2% Cu dopant used as an EPR probe of the iron spin state during thermal SCO. Distinguished the two different low-spin phases accessible in the low-spin state (Table S1).	93
$[Fe(NCS)_2(phen)_2]$	179 K; abrupt	Mn	1% Mn dopant used as an EPR probe of the iron spin state during thermal SCO.	94
$[Fe(NCS)_2(PM-BiA)_2]$	225 K; abrupt, 60 K hysteresis	Mn	A naturally occurring Mn impurity in the native iron complex was used as an EPR probe of the iron spin state during thermal SCO.	95
α-$[Fe(NCS)_2(bt)_2]$	177 K; abrupt, 10 K hysteresis	Mn	Complex also forms a second β-polymorph, which is high-spin. <5% Mn dopant used as an EPR probe of the iron spin state during thermal SCO in the α-phase.	96
$[Fe(tcnq)_2(abpt)_2]$	280 K; gradual	Mn	Trace Mn dopant used as an EPR probe of the iron spin state during thermal SCO.	97
		Cu	Trace Cu dopant used as an EPR probe of the iron spin state during thermal SCO.	97
$[Fe(pic)_3]Cl_2 \cdot EtOH$	114 and 121 K; abrupt, 2 steps	Mn	1% Mn dopant used as an EPR probe of the iron spin state during thermal SCO. The SCO transition domains observed in ref. 98 may refer to the mixed-spin intermediate phase that was subsequently discovered (*Angew. Chem. Int. Ed.*, 2003, **42**, 3825−3830).	94, 98
		Co	Co dopant used as an EPR probe of the iron spin state in the LIESST experiment.[b]	99
$[Fe(1-bpp)_2][BF_4]_2$	261 K; abrupt, 3 K hysteresis	Cu	3% Cu dopant used as an EPR probe of the iron spin state in the LIESST experiment,[b] and to probe the Jahn-Teller properties of the Cu dopant in the Fe host lattice.	100, 101
$[Fe(3-bpp)_2][BF_4]_2$	176 K; abrupt, 10 K hysteresis	Mn	3% Mn dopant used as an EPR probe of the iron spin state during thermal SCO. Demonstrated the involvement of a crystallographic phase change during the transition.	102
$[Fe(3-bpp)_2][CF_3SO_3]_2 \cdot H_2O$	215 K; abrupt, unsymmetrical 140 K hysteresis loop	Mn	3% Mn dopant used as an EPR probe of the iron spin state during thermal SCO. Demonstrated the involvement of a crystallographic phase change during the transition.	102
$[Fe(Me_23-bpp)_2][BF_4]_2$	205 K; abrupt, 65 K hysteresis	Cu	3% Cu dopant used as an EPR probe of the iron spin state during thermal SCO. Demonstrated the involvement of a symmetry-breaking phase change during the transition.	103
$[Fe(NCS)_2(\mu\text{-}btr)_2] \cdot H_2O$	134 K; abrupt, 21 K hysteresis	Mn	2D coordination polymer. 5% Mn dopant used as an EPR probe of the iron spin state during thermal SCO.	104
		Cu	1-5% Cu dopant used as an EPR probe of the iron spin state during thermal SCO.	104, 105

Table S4 continued.

Compound[a]	SCO $T_{1/2}$; form	Dopant	Notes	Refs.
[Fe(NCSe)$_2$(μ-btr)$_2$]·H$_2$O	214 K; abrupt, 7 K hysteresis	Mn	2D coordination polymer. 5% Mn dopant used as an EPR probe of the iron spin state during thermal SCO.	104
		Cu	5% Cu dopant used as an EPR probe of the iron spin state during thermal SCO.	104

[a]1-bpp = 2,6-*bis*{pyrazol-1-yl}pyridine; 3-bpp = 2,6-*bis*{1*H*-pyrazol-3-yl}pyridine; abpt = 4-amino-3,5-*bis*(pyrid-2-yl)-1,2,4-triazole; bt = 2,2'-bi(thiazoline); btr = 4,4'-bi(1,2,4-triazole); Me$_2$3-bpp = 2,6-*bis*{5-methyl-1*H*-pyrazol-3-yl}pyridine; ptz = 1-*n*-propyltetrazole; phen = 1,10-phenanthroline; pic = 2-(aminomethyl)-pyridine; PM-BiA = *N*-(2-pyridinylmethylene)[1,1'-biphenyl]-4-amine; [tcnq]$^-$ = 7,7',8,8'-tetracyanoquinodimethanide.   [b]LIESST = light-induced excited spin state trapping (ref. 143).
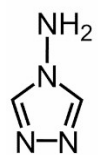

Scheme S4. Ligands listed in Table S4.

**Table S5.** Non-stoichiometric mixed-anion salts of SCO complexes, $[FeL_n]X_{2z}Y_{2-2z}$ (X^-, Y^- = anion).

Precursor compounds[a]	SCO $T_{1/2}$; form	Are the precursor salts isomorphous?	Notes	Refs.
$[Fe(Hpt)_3][BF_4]_2 \cdot 2H_2O$ $[Fe(Hpt)_3]SO_4 \cdot 3H_2O$	135 K; gradual, incomplete *ca* 100 K; gradual, incomplete	Not known	$[Fe(Hpt)_3][BF_4]_{1.2}[SO_4]_{0.4} \cdot 3H_2O$ exhibits gradual SCO with $T_{1/2}$ = 170 K, to full completeness at low temperature.	106
$[Fe(1\text{-bpp})_2][BF_4]_2$ $[Fe(1\text{-bpp})_2][ClO_4]_2$	261 K; abrupt, 3 K hysteresis High-spin	No	$[Fe(1\text{-bpp})_2][BF_4]_{2z}[ClO_4]_{2-2z}$ with $z \geq 0.5$ are fully SCO-active, with $T_{1/2}$ decreasing slightly as z decreases. The salt with z = 0.16 is a mixture of phases, and exhibits 75 %-complete SCO as a rapidly precipitate powder. The LIESST relaxation temperature is identical for all compositions.[b]	107
$[Fe(1\text{-bpp}^{NHAc})_2][BF_4]_2 \cdot EtCN$ $[Fe(1\text{-bpp}^{NHAc})_2][ClO_4]_2 \cdot EtCN$	181 and 192 K; abrupt 151 and 183 K; abrupt, 5 K and 11 K hysteresis	Yes	Stepped transition reflects a re-entrant mixed-spin crystal phase that exists at 50% conversion. $[Fe(1\text{-bpp}^{NHAc})_2][BF_4]_{2z}[ClO_4]_{2-2z} \cdot EtCN$ ($z \approx$ 0.5) exhibits the same two-step transition, with $T_{1/2}$ and hysteresis widths intermediate between the pure BF_4^- and ClO_4^- salts.	108
$[Fe(Me_23\text{-bpp})_2][BF_4]_2$ $[Fe(Me_23\text{-bpp})_2][ClO_4]_2$	205 K; abrupt, 65 K hysteresis High-spin	Yes	SCO in the BF_4^- salt involves a series of phase changes, which become kinetically slower in $[Fe(Me_23\text{-bpp})_2][BF_4]_{2z}[ClO_4]_{2-2z}$ as z increases up to 0.5. Hence the absence of SCO in the ClO_4^- salt is a kinetic effect.	109
$[Fe(\mu\text{-atrz})_3][BF_4]_2$ $[Fe(\mu\text{-atrz})_3]SiF_6$	235 K; gradual, 10 K hysteresis 248 K; gradual, 14 K hysteresis	Not known	1D coordination polymer. Various SCO behaviours were observed for different $[Fe(\mu\text{-atrz})_3][BF_4]_{2z}[SiF_6]_{1-z}$ compositions, with $T_{1/2}$ = 310 ±10 K in most samples.	110, 111
$[Fe(\mu\text{-bbtr})_3][BF_4]_2$ $[Fe(\mu\text{-bbtr})_3][ClO_4]_2$	83 K; abrupt, 13 K hysteresis 105 K; abrupt, 8 K hysteresis	Yes (at room temperature)	2D coordination polymer. The ClO_4^- salt undergoes a phase change above $T_{1/2}$ but the BF_4^- salt does not. SCO in the BF_4^- salt is kinetically slow. The slow kinetics are retained in $[Fe(\mu\text{-bbtr})_3][BF_4]_{2z}[ClO_4]_{2-2z}$ for $z \geq 0.56$, but not in more perchlorate-rich salts. The midpoint pressure of SCO at room temperature ($P_{1/2}$) varies approximately linearly with z.	112

[a] 1-bpp = 2,6-*bis*{pyrazol-1-yl}pyridine; 1-bpp^{NHAc} = *N*-(2,6-di{pyrazol-1-yl}pyrid-4-yl)acetamide; atrz = 4-amino-1,2,4-triazole; bbtr = 1,4-bis(1,2,3-triazol-1-yl)butane; Me_23-bpp = 2,6-*bis*{5-methyl-1*H*-pyrazol-3-yl}pyridine; Hpt = 3-(pyrid-2-yl)-1*H*-1,2,4-triazole. [b] LIESST = light-induced excited spin state trapping (ref. 143).
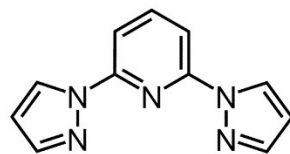
Examples of double salts of SCO complexes with stoichiometric anion compositions, $[FeL_n]XY$, are described in refs. 113-123.
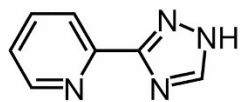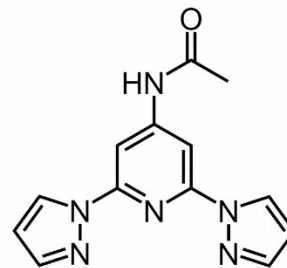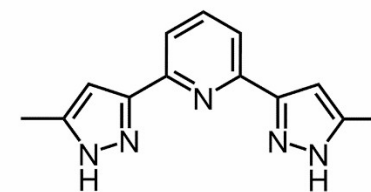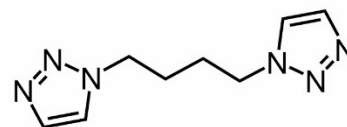
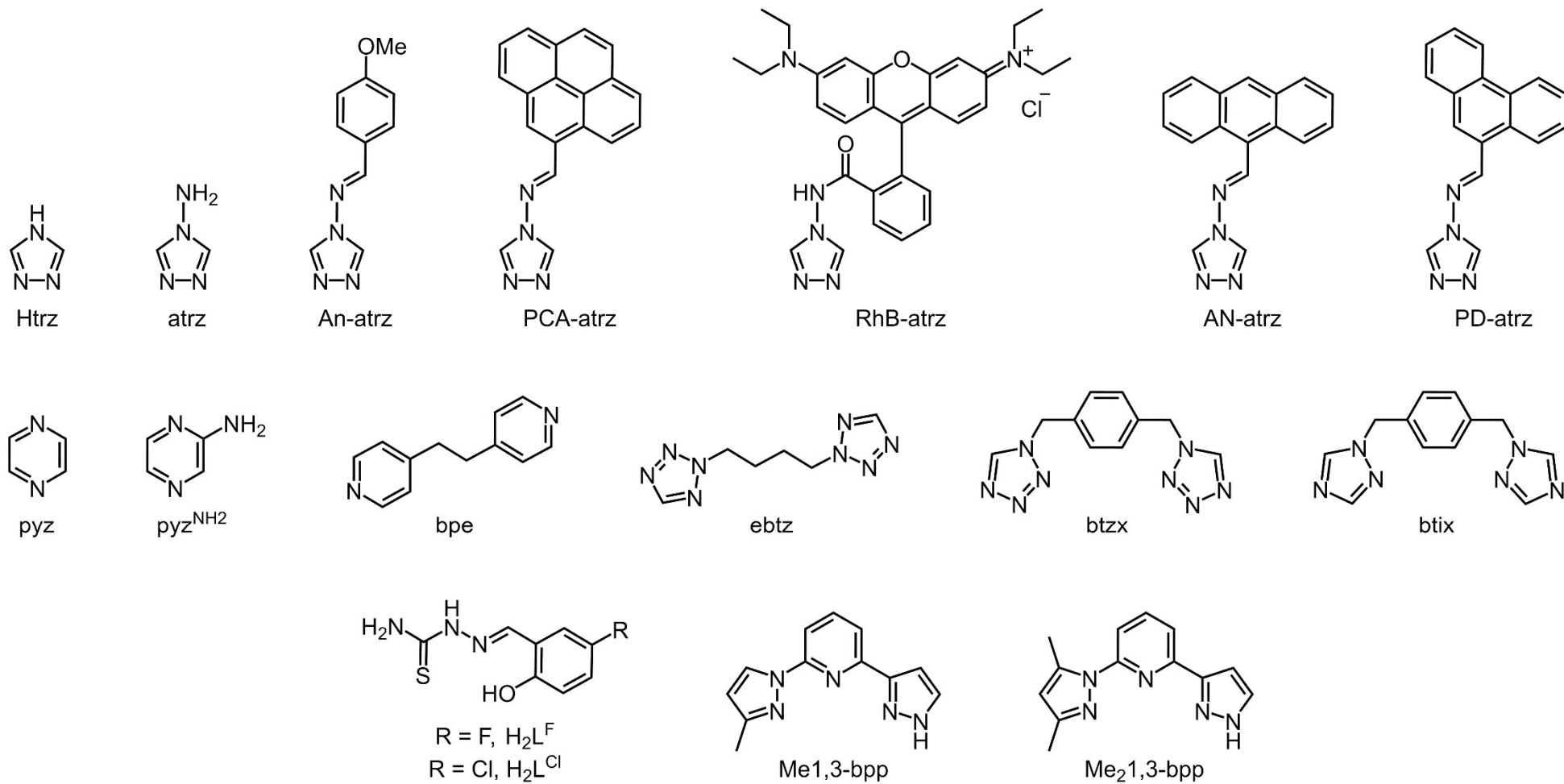**Scheme S5.** Ligands listed in Table S5.

Table S6. Molecular alloys of SCO materials, that have been characterised with non-stoichiometric compositions.

Precursor compounds[a]	SCO $T_{1/2}$; form	Are the precursors isomorphous?	Notes	Refs.
[Fe(μ-atrz)$_3$][ClO$_4$]$_2$·H$_2$O [Fe(μ-Htrz)$_3$][ClO$_4$]$_2$·H$_2$O	188 K; abrupt, 2 K hysteresis 311 K; abrupt, 15 K hysteresis	Not known	Bulk samples of [Fe(μ-atrz)$_{3n}$(μ-Htrz)$_{3-3n}$][ClO$_4$]$_2$·H$_2$O give abrupt, hysteretic SCO with $T_{1/2}$ and hysteresis width varying linearly for $0 < n < 1$. Nanoparticles of this system follow a similar trend.	124-126
[Fe(μ-atrz)$_3$][NO$_3$]$_2$ [Fe(μ-Htrz)$_3$][NO$_3$]$_2$	329 K; abrupt, 31 K hysteresis *ca* 370 K; abrupt, hysteresis	Not known	SCO in [Fe(μ-atrz)$_{3n}$(μ-Htrz)$_{3-3n}$][NO$_3$]$_2$·H$_2$O with $0 < n < 1$ becomes more abrupt as n decreases.	127
[Fe(μ-atrz)$_3$]SiF$_6$·H$_2$O [Fe(μ-Htrz)$_3$]SiF$_6$·2H$_2$O	248 K; gradual, 14 K hysteresis 404 K; gradual, irreversible	Not known	[Fe(μ-atrz)$_{3n}$(μ-Htrz)$_{3-3n}$]SiF$_6$·H$_2$O exhibit gradual SCO, with a linear dependence of $T_{1/2}$ on composition for $0 < n < 1$.	128
[Fe(μ-atrz)$_3$][BF$_4$]$_2$·H$_2$O [Fe(μ-trz)(μ-Htrz)$_2$][BF$_4$]$_2$	255 K; abrupt, 10 K hysteresis 355 K; abrupt, 40 K hysteresis	No	[Fe(μ-Htrz)$_{1+n-m}$(μ-trz)$_{2-n}$(μ-atrz)$_m$][BF$_4$]$_n$·xH$_2$O nanoparticle polymer composites show abrupt hysteretic SCO for $0 < m < 0.3$, with $T_{1/2}$ decreasing as m increases. SCO induces a strong piezoelectric response.	129-132
[Fe(μ-atrz)$_3$][NO$_3$]$_2$ [Fe(μ-An-atrz)$_3$][NO$_3$]$_2$	329 K; abrupt, 31 K hysteresis 287 K; gradual	No	Alloys produced by treating [Fe(μ-atrz)$_3$][NO$_3$]$_2$ with 4-anisylaldehyde. Intermediate compositions of [Fe(μ-atrz)$_{3n}$(μ-An-atrz)$_{3-3n}$][NO$_3$]$_2$ exhibit SCO in discrete steps, from unreacted and reacted regions of the sample.	133
[Fe(μ-atrz)$_3$][ClO$_4$]$_2$·H$_2$O [Fe(μ-PCA-atrz)$_3$][ClO$_4$]$_2$	329 K; abrupt, 31 K hysteresis Not known	Not known	[Fe(μ-atrz)$_{3n}$(μ-PCA-atrz)$_{3-3n}$][ClO$_4$]$_2$ ($n = 0.15$) produced by reacting [Fe(μ-atrz)$_3$][ClO$_4$]$_2$ and 1-pyrenecarboxaldehyde. It shows gradual SCO at 225 K with 10 K hysteresis, and spin state-dependent fluorescence.	134
[Fe(μ-atrz)$_3$][ClO$_4$]$_2$·H$_2$O [Fe(μ-RhB-atrz)$_3$][ClO$_4$]$_2$	329 K; abrupt, 31 K hysteresis Not known	Not known	[Fe(μ-atrz)$_{3n}$(μ-RhB-atrz)$_{3-3n}$][ClO$_4$]$_2$ ($n = 0.10$) produced by reacting [Fe(μ-atrz)$_3$][ClO$_4$]$_2$ and rhodamine B. It shows gradual SCO at 258 K with 11 K thermal hysteresis, and spin state-dependent fluorescence.	134
[Fe(μ-atrz)$_3$][ClO$_4$]$_2$·H$_2$O [Fe(μ-ANTH-atrz)$_3$][ClO$_4$]$_2$	329 K; abrupt, 31 K hysteresis Not known	Not known	[Fe(μ-atrz)$_{3n}$(μ-ANTH-atrz)$_{3-3n}$][ClO$_4$]$_2$ ($n = 0.13$) produced by reacting [Fe(μ-atrz)$_3$][ClO$_4$]$_2$ with 9-anthraldehyde. It shows gradual SCO at 255 K with 2 K thermal hysteresis, and spin state-dependent fluorescence.	135
[Fe(μ-atrz)$_3$][ClO$_4$]$_2$·H$_2$O [Fe(μ-PD-atrz)$_3$][ClO$_4$]$_2$	329 K; abrupt, 31 K hysteresis Not known	Not known	[Fe(μ-atrz)$_{3n}$(μ-PD-atrz)$_{3-3n}$][ClO$_4$]$_2$ ($n = 0.10$) produced by reacting [Fe(μ-atrz)$_3$][ClO$_4$]$_2$ with 9-phenanthrenecarboxaldehyde. It shows gradual SCO at 255 K with 2 K thermal hysteresis, and spin state-dependent fluorescence.	135

Table S6 continued.

Precursor compounds[a]	SCO $T_{1/2}$; form	Are the precursors isomorphous?	Notes	Refs.
[Fe(μ-pyz){Pd(CN)$_4$}] [Fe(μ-pyz^{NH_2}){Pd(CN)$_4$}]	296 K; abrupt, 12 K hysteresis High-spin	No	SCO in [Fe(μ-pyz)$_n$(μ-pyz^{NH_2})$_{1-n}${Pd(CN)$_4$}] has lower $T_{1/2}$ as n decreases, in the range $0.3 < n < 1$. The transition also becomes increasingly gradual, with narrower hysteresis, for lower values of n.	136
[Fe(μ-pyz){Pt(CN)$_4$}] [Fe(μ-pyz^{NH_2}){Pt(CN)$_4$}]	295 K; abrupt, 26 K hysteresis High-spin	No	SCO in [Fe(μ-pyz)$_n$(μ-pyz^{NH_2})$_{1-n}${Pt(CN)$_4$}] shows lower $T_{1/2}$ and narrower hysteresis as n decreases, for $0.6 < n < 1$. The relationship between $T_{1/2}$ vs. composition is approximately linear. Alloys with $n \leq 0.5$ are high-spin.	136
[Fe(μ-pyz){Pt(CN)$_4$}] [Fe(μ-pyz){PtI$_2$(CN)$_4$}]	295 K; abrupt, 26 K hysteresis 390 K; abrupt, 17 K hysteresis	Yes	Alloys produced by reaction of [Fe(μ-pyz){Pt(CN)$_4$}] with I$_2$. [Fe(μ-pyz){PtI$_2$(CN)$_4$}$_n${Pt(CN)$_4$}$_{1-n}$] ($0 < n < 1$) exhibit consistently hysteretic spin-transitions, with $T_{1/2}$ increasing linearly with n.	137
[Fe(NCEt)$_2$(μ-ebtz)$_2$][BF$_4$]$_2$ [Fe(NCPr)$_2$(μ-ebtz)$_2$][BF$_4$]$_2$	101 K; abrupt, 41 K hysteresis 190 K; gradual	Yes	SCO in the EtCN complex is only observed upon slow thermal scanning. In [Fe(NCEt)$_{2n}$(NCPr)$_{2-2n}$(μ-ebtz)$_2$][BF$_4$]$_2$ ($0.72 \leq n < 1$) $T_{1/2}$ increases and the hysteresis narrows with larger PrCN content.	138
[Fe(μ-btzx)$_3$][ClO$_4$]$_2$ [Fe(μ-btix)$_3$][ClO$_4$]$_2$	200 K; gradual High-spin	No	Compositions of [Fe(μ-btix)$_{3n}$(μ-btzx)$_{3-3n}$][ClO$_4$]$_2$ with $n \leq 0.2$ undergo gradual, incomplete SCO in two or three resolvable steps.	139
[Fe(NCS)$_2$(μ-bpe)$_2$]·solvent [Fe(NCBH$_3$)$_2$(μ-bpe)$_2$]·solvent	84 K; abrupt 216 K; abrupt	No	Two compositions of [Fe(NCS)$_{2n}$(NCBH$_3$)$_{2-2n}$(μ-bpe)$_2$]·solvent with $n \geq 0.8$ undergo gradual SCO in two resolvable steps.	140
[Fe(L^F)(HL^F)]·H$_2$O [Fe(L^{Cl})(HL^{Cl})]·H$_2$O	317 K; abrupt 230 K; abrupt	No	$T_{1/2}$ increases non-linearly for [Fe(H$_{0.5}$L^F)$_{2n}$(H$_{0.5}$L^{Cl})$_{2-2n}$]·H$_2$O ($0 < n < 1$). SCO is abrupt for $n < 0.2$ and $n > 0.8$, but broadens as n approaches 0.5.	141
[Fe(Me$_2$1,3-bpp)$_2$][ClO$_4$]$_2$ [Fe(Me1,3-bpp)$_2$][ClO$_4$]$_2$	378 K; gradual 184 K; abrupt	No	SCO in [Fe(Me$_2$1,3-bpp)$_{2n}$(Me1,3-bpp)$_{2-2n}$][ClO$_4$]$_2$ ($n \leq 0.5$) shifts linearly to higher temperature and becomes more gradual as n increases. Samples with $n > 0.5$ were mixed phase materials.	142

[a]An-atrz = N-[(4-methoxyphenyl)methylene]-4H-1,2,4-triazol-4-amine; ANTH-atrz = N-[(anthr-9-yl)methylene]-4H-1,2,4-triazol-4-amine; atrz = 4-amino-1,2,4-triazole; bpe = 1,2-*bis*(pyrid-4-yl)ethane; btix = 1,4-*bis*(1,2,4-triazol-1-ylmethyl)benzene; btzx = 1,4-*bis*(tetrazol-1-ylmethyl)benzene; ebtz = 1,2-*bis*(tetrazol-2-yl)ethane; H$_2$L^{Cl} = 2-({5-chloro-2-hydroxyphenyl}methylene)hydrazinecarbothioamide; H$_2$L^F = 2-({5-fluoro-2-hydroxyphenyl}methylene)hydrazinecarbothioamide; Me1,3-bpp = 2-(3-methylpyrazol-1-yl)-6-(1H-pyrazol-3-yl)pyridine; Me$_2$1,3-bpp = 2-(3,5-dimethylpyrazol-1-yl)-6-(1H-pyrazol-3-yl)pyridine; PCA-atrz = N-[(pyren-1-yl)methylene]-4H-1,2,4-triazol-4-amine; PD-atrz = N-[(phenanthren-9-yl)methylene]-4H-1,2,4-triazol-4-amine; pyz = pyrazine; pyz^{NH_2} = aminopyrazine; RhB-atrz = 3,6-*bis*(diethylamino)-9-(2-{[4H-1,2,4-triazol-4-ylamino]carbonyl}phenyl)xanthylium chloride; Htrz = 4H-1,2,4-triazole.

Scheme S6. Ligands listed in Table S6.

References

1. P. Ghosh, C. M. Pask, H. B. Vasili, N. Yoshinari, T. Konno, O. Cespedes, C. Enachescu, P. Chakraborty and M. A. Halcrow, *J. Mater. Chem. C*, 2023, **11**, 12570–12582.

2. C. Baldé, C. Desplanches, F. Le Gac, P. Guionneau and J.-F. Létard, *Dalton Trans.*, 2014, **43**, 7820–7829.

3. C. Baldé, C. Desplanches, J.-F. Létard and G. Chastanet, *Polyhedron*, 2017, **123**, 138–144.

4. C. Baldé, C. Desplanches, P. Gütlich, E. Freysz and J.-F. Létard, *Inorg. Chim. Acta*, 2008, **361**, 3529–3533.

5. P. Ganguli, P. Gütlich and E. W. Müller, *Inorg. Chem.*, 1982, **21**, 3429–3433.

6. C. Baldé, C. Desplanches, A. Wattiaux, P. Guionneau, P. Gütlich and J.-F. Létard, *Dalton Trans.*, 2008, 2702–2707.

7. M. S. Sylla, C. Baldé, N. Daro, C. Desplanches, M. Marchivie and G. Chastanet, *Eur. J. Inorg. Chem.*, 2018, 297–304.

8. T. Buchen, P. Poganiuch and P. Gütlich, *J. Chem. Soc. Dalton Trans.*, 1994, 2285–2288.

9. T. Buchen, D. Schollmeyer and P. Gütlich, *Inorg. Chem.*, 1996, **35**, 155–161.

10. E. W. Müller, J. Ensling, H. Spiering and P. Gütlich, *Inorg. Chem.*, 1983, **22**, 2074–2078.

11. A. Hauser, P. Gütlich and H. Spiering, *Inorg. Chem.*, 1986, **25**, 4245–4248.

12. J. Jung, G. Schmitt, L. Wiehl, A. Hauser, K. Knorr, H. Spiering and P. Gütlich, *Z. Phys. B*, 1996, **100**, 523–534.

13. J. Jeftić and A. Hauser, *J. Phys. Chem. B*, 1997, **101**, 10262–10270.

14. J. Kusz, H. Spiering and P. Gütlich, *J. Appl. Cryst.*, 2004, **37**, 589–595.

15. P. Chakraborty, M. Sy, H. Fourati, T. Delgado, M. Dutta, C. Das, C. Besnard, A. Hauser, C. Enachescu and K. Boukheddaden, *Phys. Chem. Chem. Phys.*, 2022, **24**, 982–994.

16. F. J. Valverde-Muñoz, R. G. Torres Ramírez, A. Ulhe, E. Trzop, M. Dutta, C. Das, P. Chakraborty and E. Collet, *CrystEngComm*, 2023, **25**, 3588–3597.

17. G. Lebedev, S. Pillet, C. Baldé, P. Guionneau, C. Desplanches and J.-F. Létard, *IOP Conf. Ser.: Mater. Sci. Eng.*, 2009, **5**, 012025.

18. S. Saha, P. Chandra and S. K. Mandal, *Physica B*, 2022, **642**, 414128.

19. N. Paradis, G. Chastanet, T. Palamarciuc, P. Rosa, F. Varret, K. Boukheddaden and J.-F. Létard, *J. Phys. Chem. C*, 2015, **119**, 20039–20050.

20. P. Adler, L. Wiehl, E. Meibner, C. P. Köhler, H. Spiering and P. Gütlich, *J. Phys. Chem. Solids*, 1987, **48**, 517–525.

21. P. Gütlich, R. Link and H. G. Steinhauser, *Inorg. Chem*, 1978, **17**, 2509–2514.

22. H. Spiering, E. Meissner, H. Köppen, E. W. Müller and P. Gütlich, *Chem. Phys.*, 1982. **68**, 65–71.

23. E. Meissner, H. Köppen, H. Spiering and P. Gütlich, *Chem. Phys. Lett.*, 1983, **95**, 163–166.

24. R. Jakobi, H. Spiering, L. Wiehl, E. Gmelin and P. Gütlich, *Inorg. Chem*, 1988, **27**, 1823–1827.

25. C. P. Köhler, R. Jakobi, E. Meissner, L. Wiehl, H. Spiering and P. Gütlich, *J. Phys. Chem. Solids*, 1990, **51**, 239–247.

26. R. Jakobi, H. Spiering and P. Gütlich, *J. Phys. Chem. Solids*, 1992, **53**, 267–275.

27. T. Kohlhaas, H. Spiering and P. Gütlich, *Z. Phys. B*, 1997, **102**, 455–459.

28. I. Sanner, E. Meissner, H. Köppen, H. Spiering and P. Gütlich, *Chem. Phys.*, 1984, **86**, 227–233.

29. C. M. Pask. A. N. Kulak and M. A. Halcrow, *Eur. J. Inorg. Chem.*, doi: 10.1002/ejic.202400334.

30. M. A. Halcrow and G. Chastanet, *Polyhedron*, 2017, **136**, 5–12.

31. C. A. Tovee, C. A. Kilner, J. A. Thomas and M. A. Halcrow, *CrystEngComm*, 2009, **11**, 2069–2077.

32. M. A. Halcrow, H. B. Vasili, C. M. Pask. A. N. Kulak and O. Cespedes, *Dalton Trans.*, 2024, **53**, 6983–6992.

33. V. García-López, F. J. Orts-Mula, M. Palacios-Corella, J. M. Clemente-Juan, M. Clemente-León and E. Coronado, *Polyhedron*, 2018, **150**, 54–60.

34. N. Paradis, G. Chastanet and J.-F. Létard, *Eur. J. Inorg. Chem.*, 2012, 3618–3624.

35. N. Paradis, G. Chastanet, F. Varret and J.-F. Létard, *Eur. J. Inorg. Chem.*, 2013, 968–974.

36. R. Diego, O. Roubeau and G. Aromí, *Chem. Sq.*, 2021, 5–1.

37. Z. Yu, T. Kuroda-Sowa, H. Kume, T. Okubo, M. Maekawa and M. Munakata, *Bull. Chem. Soc. Jpn.*, 2009, **82**, 333–337.

38. S. Zheng, M. A. Siegler, J. S. Costa, W.-T. Fu and S. Bonnet, *Eur. J. Inorg. Chem.*, 2013, 1033–1042.

39. X. Li, D. Zhang, Y. Qian, W. Liu, C. Mathonière, R. Clérac and X. Bao, *J. Am. Chem. Soc.*, 2023, **145**, 9564−9570.

40. B. Drahoš, I. Šalitroš, I. Císařová and R. Herchel, *Dalton Trans.*, 2021, **50**, 11147–11157.

41. H. Wang, C. Baldé, A. Grosjean, C. Desplanches, P. Guionneau and G. Chastanet, *Dalton Trans.*, 2018, **47**, 14741–14750.

42. P. Chakraborty, A. Tissot, L. Peterhans, L. Guénée, C. Besnard, P. Pattison and A. Hauser, *Phys. Rev. B*, 2013, **87**, 214306.

43. T. Delgado and A.-L. Pelé, *Crystals*, 2024, **14**, 210.

44. A. B. Gaspar, V. Ksenofontov, S. Reiman, P. Gütlich, A. L. Thompson, A. E. Goeta, M. C. Muñoz and J. A. Real, *Chem. – Eur. J.*, 2006, **12**, 9289–9298.

45. A. Moneo-Corcuera, D. Nieto-Castro, J. Cirera, V. Gómez, J. Sanjosé-Orduna, C. Casadevall, G. Molnár, A. Bousseksou, T. Parella, J. M. Martínez-Agudo, J. Lloret-Fillol, M. H. Pérez-Temprano, E. Ruiz and J. R. Galán-Mascarós, *Chem*, 2023, **9**, 377–393.

46. R. Ohtani, S. Egawa, M. Nakaya, H. Ohmagari, M. Nakamura, L. F. Lindoy and S. Hayami, *Inorg. Chem.*, 2016, **55**, 3332–3337.

47. S. Hayami, D. Urakami, Y. Kojima, H. Yoshizaki, Y. Yamamoto, K. Kato, A. Fuyuhiro, S. Kawata and K. Inoue, *Inorg. Chem.*, 2010, **49**, 1428–1432.

48. L. G. Lavrenova, V. N. Ikorskii, V. A. Varnek, I. M. Oglezneva and S. V. Larionov, *J. Struct. Chem.*, 1993, **34**, 960–965.

49. V. A. Varnek and L. G. Lavrenova, *J. Struct. Chem.*, 1994, **35**, 842–850.

50. V. A. Varnek and L. G. Lavrenova, *J. Struct. Chem.*, 1995, **36**, 97–103.

51. S. B. Erenburg, N. V. Bausk, V. A. Varnek and L. G. Lavrenova, *J. Magn. Magn. Mater.*, 1996, **157–158**, 595–596.

52. S. B. Erenburg, N. V. Bausk, L. G. Lavrenova, V. A. Varnek and L. N. Mazalov, *Solid State Ionics*, 1997, **101–103**, 571–577.

53. V. A. Varnek and L. G. Lavrenova, *J. Struct. Chem.*, 1997, **38**, 850–852.

54. Yu. G. Shvedenkov, V. N. Ikorskii, L. G. Lavrenova, V. A. Drebushchak and N. G. Yudina, *J. Struct. Chem.*, 1997, **38**, 578–584.

55. V. A. Varnek, L. G. Lavrenova and S. A. Gromilov, *J. Struct. Chem.*, 1997, **38**, 585–592.

56. K. Jenni, L. Scherthan, I. Faus, J. Marx, C. Strohm, M. Herlitschke, H.-C. Wille, P. Würtz, V. Schünemann and J. A. Wolny, *Phys. Chem. Chem. Phys.*, 2017, **19**, 18880–18889.

57. O. G. Shakirova, Yu. G. Shvedenkov, D. Yu. Naumov, N. F. Beizel', L. A. Sheludyakova, L. S. Dovlitova, V. V. Malakhov and L. G. Lavrenova, *J. Struct. Chem.*, 2002, **43**, 601–607.

58. E. Coronado, J. R. Galán-Mascarós, M. Monrabal-Capilla, J. García-Martínez and P. Pardo-Ibáñez, *Adv. Mater.*, 2007, **19**, 1359–1361.

59. J. R. Galán-Mascarós, E. Coronado, A. Forment-Aliaga, M. Monrabal-Capilla, E. Pinilla-Cienfuegos and M. Ceolin, *Inorg. Chem.*, 2010, **49**, 5706–5714.

60. S. Titos-Padilla, J. M. Herrera, X.-W. Chen, J. J. Delgado and E. Colacio, *Angew. Chem. Int. Ed.*, 2011, **50**, 3290–3293.

61. C. Lefter, S. Tricard, H. Peng, G. Molnár, L. Salmon, P. Demont, A. Rotaru and A. Bousseksou, *J. Phys. Chem. C*, 2015, **119**, 8522–8529.

62. C. Baldé, C. Desplanches, M. Grunert, Y. Wei, P. Gütlich and J.-F. Létard, *Eur. J. Inorg. Chem.*, 2008, 5382–5389.

63. C. Baldé, M. S. Sylla, C. Desplanches and G. Chastanet, *Polyhedron*, 2019, **159**, 84–92.

64. R. Tanasa, C. Enachescu, A. Stancu, J. Linarès, E. Codjovi, F. Varret and J. Haasnoot, *Phys. Rev. B*, 2005, **71**, 014431.

65. R. Tanasa, C. Enachescu, A. Stancu, F. Varret, J. Linarès and E. Codjovi, *Polyhedron*, 2007, **26**, 1820–1824.

66. A. Rotaru, M. M. Dîrtu, C. Enachescu, R. Tanasa, J. Linarès, A. Stancu and Y. Garcia, *Polyhedron*, 2009, **28**, 2531–2536.

67. J.-P. Martin, J. Zarembowitch, A. Dworkin, J. G. Haasnoot and E. Codjovi, *Inorg. Chem.,* 1994, **33**, 2617–2623.

68. E. Codjovi, N. Menéndez, J. Jeftic and F. Varret, *C. R. Acad. Sci. Chim.*, 2001, **4**, 181–188.

69. N. Nègre, C. Conséjo, M. Goiran, A. Bousseksou, F. Varret, J.-P. Tuchagues, R. Barbaste, S. Askénazy and J. G. Haasnoot, *Physica B*, 2001, **294–295**, 91–95.

70. C. Enachescu, J. Linarès and F. Varret, *J. Phys.: Condens. Matter*, 2001, **13** 2481–2495.

71. J.-P. Martin, J. Zarembowitch, A. Bousseksou, A. Dworkin, J. G. Haasnoot and F. Varret, *Inorg. Chem.*, 1994, **33**, 6325–6333.

72. A. Desaix, O. Roubeau, J. Jeftic, J.G. Haasnoot, K. Boukheddaden, E. Codjovi, J. Linarès, M. Noguès and F. Varret, *Eur. Phys. J. B*, 1998, **6**, 183–193.

73. J. Kusz, R. Bronisz, M. Zubko and G. Bednarek, *Chem. – Eur. J.*, 2011, **17**, 6807–6820.

74. P. Chakraborty, C. Enachescu, C,Walder, R. Bronisz and A. Hauser, *Inorg. Chem.*, 2012, **51**, 9714–9722.

75. P. Chakraborty, C. Enachescu and A. Hauser, *Eur. J. Inorg. Chem.*, 2013, 770–780.

76. P. Chakraborty, C. Enachescu, A. Humair, L. Egger, T. Delgado, A. Tissot, L. Guénée, C. Besnard, R. Bronisz and A. Hauser, *Dalton Trans.,* 2014, **43**, 17786–17796.

77. R.-M. Stan, R. Gaina, C. Enachescu, R. Tanasa, A. Stancu and R. Bronisz, *J. Appl. Phys.*, 2015, **117**, 17B323.

78. C. Das, S. Dey, A. Adak, C. Enachescu and P. Chakraborty, *Cryst. Growth Des.*, 2023, **23**, 3496–3508.

79. M. S. Sylla, C. Baldé, N. Daro and G. Chastanet, *J. Soc. Ouest-Afr. Chim.*, 2017, **43**, 37–47.

80. T. Tayagaki, A. Galet, G. Molnár, M. C. Muñoz, A. Zwick, K. Tanaka, J.-A. Real and A. Bousseksou, *J. Phys. Chem. B*, 2005, **109**, 14859–14867.

81. Y. Avila, R. Terrero, P. M. Crespo, L. A. Diaz-Paneque, M. Gonzalez, M. Avila and E. Reguera, *Eur. J. Inorg. Chem.*, 2021, 3969–3980.

82. B. R. Mullaney, L. Goux-Capes, D. J. Price, G. Chastanet, J.-F. Létard and C. J. Kepert, *Nat. Commun.*, 2017, **8**, 1053.

83. J.-S. M. Lee, Y. Fujiwara, S. Kitagawa and S. Horike, *Chem. Mater.*, 2019, **31**, 4205–4212.

84. K. Bode, P. Gütlich and H. Köppen, *Inorg. Chim. Acta*, 1980, **42**, 281–284.

85. A. Hauser, *Chem. Phys. Lett.*, 1990, **173**, 507–512.

86. S. Schenker, A. Hauser, W. Wang and I. Y. Chan, *Chem. Phys. Lett.*, 1998, **297**, 281–286.

87. A. Hauser, N. Amstutz, S. Delahaye, A. Sadki, S. Schenker, R. Sieber and M. Zerara, *Struct. Bonding (Berlin)*, 2004, **106**, 81–96.

88. A. Vef, U. Manthe, P. Gütlich and A. Hauser, *J. Chem. Phys.*, 1994, **101**, 9326–9332.

89. F. Renz, H. Oshio, V. Ksenofontov, M. Waldeck, H. Spiering and P. Gütlich, *Angew. Chem. Int. Ed.*, 2000, **39**, 3699–3700.

90. S. Schenker, A. Hauser, W. Wang and I. Y. Chan, *J. Chem. Phys.*, 1998, **109**, 9870–9878.

91. I. Krivokapic, P. Chakraborty, R. Bronisz, C. Enachescu and A. Hauser, *Angew. Chem. Int. Ed.*, 2010, **49**, 8509–8512.

92. I. Krivokapic, P. Chakraborty, C. Enachescu, R. Bronisz and A. Hauser, *Inorg. Chem.*, 2011, **50**, 1856–1861.

93. A. Ozarowski and B. R. McGarvey, *Inorg. Chem.*, 1989, **28**, 2262–2266.

94. P. S. Rao, A. Reuveni, B. R. McGarvey and P. Gütlich, *Inorg. Chem.*, 1981, **20**, 204–207.

95. H. Daubric, J. Kliava, P. Guionneau, D. Chasseau, J.-F. Létard and O. Kahn, *J. Phys.: Condens. Matter*, 2000, **12**, 5481–5494.

96. A. Ozarowski, B. R. McGarvey, A. B. Sarkar and J. E. Drake, *Inorg. Chem.,* 1988, **27**, 628–635 and 1988, **27**, 2560 (correction).

97. P. J. Kunkeler, P. J. van Koningsbruggen, J. P. Cornelissen, A. N. van der Horst, A. M. van der Kraan, A. L. Spek, J. G. Haasnoot and J. Reedijk, *J. Am. Chem. Soc.*, 1996, **118**, 2190–2197.

98. P. E. Doan and B. R. McGarvey, *Inorg. Chem.,* 1990, **29**, 874–876.

99. M. Shirai, N. Yonemura, T. Tayagaki, K. Kan'no, K. Tanaka, *J. Luminesc.*, 2001, **94–95**, 529–532.

100. R. Docherty, F. Tuna, C. A. Kilner, E. J. L. McInnes and M. A. Halcrow, *Chem. Commun.,* 2012, **48**, 4055–4057.

101. S. V. Tumanov, S. L. Veber, S. Greatorex, M. A. Halcrow and M. V. Fedin, *Inorg. Chem.*, 2018, **57**, 8709−8713.

102. R. C. W. Sung and B. R. McGarvey, *Inorg. Chem.*, 1999, **38**, 3644–3650.

103. C. M. Pask, S. Greatorex, R. Kulmaczewski, A. Baldansuren, E. J. L. McInnes, F. Bamiduro, M. Yamada, N. Yoshinari, T. Konno and M. A. Halcrow, *Chem. – Eur. J.*, 2020, **26**, 4833–4841.

104. A. Ozarowski, Y. Shunzhong, B. R. McGarvey, A. Mislankar and J. E. Drake, *Inorg. Chem.*, 1991, **30**, 3167–3174.

105. W. Vreugdenhil, J. G. Haasnoot, O. Khan, P. Thuéry and J. Reedijk, *J. Am. Chem. Soc.*, 1987, **109**, 5272–5273.

106. O. Roubeau, M. de Vos, A.F. Stassen, R. Burriel, J. G. Haasnoot and J. Reedijk, *J. Phys. Chem. Solids*, 2003, **64**, 1003–1013.

107. C. Carbonera, C. A. Kilner, J.-F. Létard and M. A. Halcrow, *Dalton Trans.*, 2007, 1284–1292.

108. I. Capel Berdiell, R. Kulmaczewski, N. Shahid, O. Cespedes and M. A. Halcrow, *Chem. Commun.*, 2021, **57**, 6566–6569.

109. T. D. Roberts, C. M. Pask, I. Capel Berdiell, F. Tuna and M. A. Halcrow, *J. Mater. Chem. C*, 2022, **10**, 16353–16362.

110. X. Yang, A. Enriquez-Cabrera, D. Toha, Y. Coppel, L. Salmon and A. Bousseksou, *Dalton Trans.*, 2023, **52**, 10828–10834.

111. X. Yang, A. Enriquez-Cabrera, K. Jacob, Y. Coppel, L. Salmon and A. Bousseksou, *Dalton Trans.*, 2024, **53**, 6830–6838.

112. M. Książek, M. Weselski, M. Kaźmierczak, A. Półrolniczak, A. Katrusiak, D. Paliwoda, J. Kusz and R. Bronisz, *Chem. − Eur. J.*, 2024, **30**, e202302887.

113. E. Coronado, M. C. Giménez-López, C. Gimenez-Saiz, J. M. Martínez-Agudo and F. M. Romero, *Polyhedron*, 2003, **22**, 2375–2380.

114. M. Yamada, H. Hagiwara, H. Torigoe, N. Matsumoto, M. Kojima, F. Dahan, J.-P. Tuchagues, N. Re and S. Iijima, *Chem. − Eur. J.*, 2006, **12**, 4536–4549.

115. H. Hagiwara, N. Matsumoto, S. Iijima and M. Kojima, *Inorg. Chim. Acta*, 2011, **366**, 283–289.

116. K. Nishi, N. Matsumoto, S. Iijima, M. A. Halcrow, Y. Sunatsuki and M. Kojima, *Inorg. Chem.*, 2011, **50**, 11303–11305.

117. K. Nishi, H. Kondo, T. Fujinami, N. Matsumoto, S. Iijima, M. A. Halcrow, Y. Sunatsuki and M. Kojima, *Eur. J. Inorg. Chem.*, 2013, 927–933.

118. T. Fujinami, K. Nishi, D. Hamada, K. Murakami, N. Matsumoto, S. Iijima, M. Kojima and Y. Sunatsuki, *Inorg. Chem.*, 2015, **54**, 7291–7300.

119. H. Phan, S. M. Benjamin, E. Steven, J. S. Brooks and M. Shatruk, *Angew. Chem. Int. Ed.*, 2015, **54**, 823–827.

120. W. Phonsri, B. A. I. Lewis, G. N. L. Jameson and K. S. Murray, *Chem. Commun.,* 2019, **55**, 14031–14034.

121. M. D. Darawsheh, L. A. Barrios, O. Roubeau, S. J. Teat and G. Aromí, *Chem. Commun.,* 2017, **53**, 569–572.

122. M. Darawsheh, L. A. Barrios, O. Roubeau, S. J. Teat and G. Aromí, *Angew. Chem. Int. Ed.*, 2018, **57**, 13509–13513.

123. N. Capó, L. A. Barrios, J. Cardona, J. Ribas-Ariño, S. J. Teat, O. Roubeau and G. Aromí, *Chem. Commun.*, 2022, **58**, 10969–10972.

124. O. Kahn, L. Sommier and E. Codjovi, *Chem. Mater.*, 1997, **9***, 3199–3205.

125. O. Kahn and C. Jay Martinez, *Science*, 1998, **279**, 44–48.

126. M. Giménez-Marqués, M. L. García-Sanz de Larrea and E. Coronado, *J. Mater. Chem. C*, 2015, **3**, 7946–7953.

127. O. G. Shakirova, L. G. Lavrenova, Yu. G. Shvedenkov, V. N. Ikorskii, V. A. Varnek, L. A. Sheludyakova, V. L. Varand, T. A. Krieger, and S. V. Larionov, *J. Struct. Chem.*, 2000, **41**, 790–797.

128. O. G. Shakirova, M. Grunert, D. Yu. Naumov, P. Gütlich and L. G. Lavrenova *J. Struct. Chem.*, 2010, **51**, 45–52.

129. S. Rat, M. Piedrahita-Bello, L. Salmon, G. Molnár, P. Demont and A. Bousseksou, *Adv. Mater.*, 2018, **30**, 1705275.

130. M. Piedrahita-Bello, K. Ridier, M. Mikolasek, G. Molnár, W. Nicolazzi, L. Salmon and A. Bousseksou, *Chem. Commun.*, 2019, **55**, 4769–4772.

131. M. Piedrahita-Bello, B. Martin, L. Salmon, G. Molnár, P. Demont and A. Bousseksou, *J. Mater. Chem. C*, 2020, **8**, 6042–6051.

132. I. Soroceanu, S.-L. Lupu, I. Rusu, M. Piedrahita-Bello, L. Salmon, G. Molnár, P. Demont, A. Bousseksou and A. Rotaru, *J. Phys.: Condens. Matter,* 2020, **32**, 264002.

133. A. Enríquez-Cabrera, L. Routaboul, L. Salmon and A. Bousseksou, *Dalton Trans.*, 2019, **48**, 16853–16856.

134. C.-F. Wang, R.-F. Li, X.-Y. Chen, R.-J. Wei, L.-S. Zheng and J. Tao, *Angew. Chem. Int. Ed.*, 2015, **54**, 1574–1577.

135. C.-F. Wang, G.-Y. Yang, Z.-S. Yao and J. Tao, *Chem. − Eur. J.*, 2018, **24**, 3218–3224.

136. Y. Gong, Z.-H. Li, X. Yan, Y.-Q. Wang, C.-Y. Zhao, W.-K. Han, Q.-T. Hu, H.-S. Lu and Z.-G. Gu, *Chem. – Eur. J.*, 2020, **26**, 12472–12480.

137. R. Ohtani, K. Yoneda, S. Furukawa, N. Horike, S. Kitagawa, A. B. Gaspar, M. C. Muñoz, J. A. Real and M. Ohba, *J. Am. Chem. Soc.*, 2011, **133**, 8600–8605.

138. M. Książek, M. Weselski, M. Kaźmierczak, A. Tołoczko, M. Siczek, P. Durlak, J. A. Wolny, V. Schünemann, J. Kusz and R. Bronisz, *Chem. – Eur. J.*, 2020, **26**, 14419–14434.

139. N. C. Galve, E. Coronado, M. Giménez-Marqués and G. M. Espallargas, *Inorg. Chem.*, 2014, **53**, 4482–4490.

140. H. Dote, M. Kaneko, K. Inoue and S. Nakashima, *Bull. Chem. Soc. Jpn.*, 2018, **91**, 71–81.

141. Y.-Y. Wu, Z.-Y. Li, S. Peng, Z.-Y. Zhang, H.-M. Cheng, H. Su, W.-Q. Hou, F.-L. Yang, S.-Q. Wu, O. Sato, J.-W. Dai, W. Li and X.-H. Bu, *J. Am. Chem. Soc.*, 2024, **146**, 8206−8215.

142. C. Bartual-Murgui, C. Pérez-Padilla, S. J. Teat, O. Roubeau and G. Aromí, *Inorg. Chem.*, 2020, **59**, 12132–12142.

143. a) D. Unruh, P. Homenya, M. Kumar, R. Sindelar, Y. Garcia and F. Renz, *Dalton Trans.*, 2016, **45**, 14008–14018;
    b) G. Chastanet, C. Desplanches, C. Baldé, P. Rosa, M. Marchivie and P. Guionneau, *Chem. Sq.*, 2018, 2–2.

144. a) M. Marchivie, P. Guionneau, J.-F. Létard, D. Chasseau and J. A. K. Howard, *J. Phys. Chem. Solids*, 2004, **65**, 17–23;
    b) G. A. Craig, J. S. Costa, S. J. Teat, O. Roubeau, D. S. Yufit, J. A. K. Howard and G. Aromí, *Inorg. Chem.*, 2013, **52**, 7203–7209.

145. a) G. A. Craig and M. Murrie, *Chem. Soc. Rev.,* 2015, **44**, 2135–2147;
    b) A. Sarkar, S. Dey and G. Rajaraman, *Chem. – Eur. J.*, 2020, **26**, 14036–14058.

146. S. Hayami, M. R. Karim and Y. H. Lee, *Eur. J. Inorg. Chem.*, 2013, 683–696.